Possible Spreadings of Buoyant Plumes and Local Coastline Sensitivities Using Flow Syntheses From 1992 to 2007

Ross Tulloch, Chris Hill, and Oliver Jahn

Department of Earth, Atmospheric and Planetary Sciences, Massachusetts Institute of Technology, Cambridge, Massachusetts, USA

We present results from an ensemble of simulations where a buoyant dye is injected at the site of the *Deepwater Horizon* blowout from April 20 to July 15 of each year between 1992 and 2007. Ocean currents are taken from observationally constrained Estimating the Circulation and Climate of the Ocean Phase 2 (ECCO2) project state estimates spanning 1992 to 2007. Starting from this basis, we explore the utility of adjoint equations in allowing proactive evaluation of regional impact likelihood. Forward integrations are performed to assess the ensemble spread of the plume, the role of increased resolution of ocean eddies, and to compare spreading metrics using an Eulerian tracer and Lagrangian particles. Spreading statistics compare well with previous studies, and the Lagrangian and Eulerian approaches predict similar spreading rates, allowing some confidence in adjoint sensitivity analysis of the vulnerability of different local coastline regions to be conducted. Example adjoint calculations indicate that coastline of the Mississippi Delta is most sensitive to spills on the continental shelf off adjacent to Mississippi and Alabama, while Cape Hatteras, for example, is most sensitive to spills on the continental shelf from Delaware to South Carolina. Combined with accurate estimates of historical currents and winds, we argue that the adjoint approach we describe can be a useful regional planning and preparedness tool. Using the adjoint approach, local communities can proactively identify spill locations to which they are especially vulnerable, allowing for better preparedness and more efficient response to any future incidents.

1. INTRODUCTION

Prompted by the oil well blowout that occurred beneath the *Deepwater Horizon* drilling platform in the Gulf of Mexico on 20 April 2010, we performed a series of simulations to determine both the likely spread of oil from the spill site (forward calculations) and the sensitivity of various coastal locations to pollutants injected anywhere into the ocean (using backward, or adjoint, calculations). During the 2010 spill, there was considerable uncertainty around the likely areas of impact. Coastal communities all along the U.S. east coast and around the Gulf of Mexico were concerned that their coastline would be impacted.

A variety of modeling studies, for example, the works of *Adcroft et al.* [2010], *Maltrud et al.* [2010], *Barker* [this volume], *Ji et al.* [this volume], *Weisberg et al.* [this volume], and *Liu et al.* [this volume(a), this volume(b)], attempted to quantify the uncertain impacts by modeling plumes spreading from the blowout using one or more circulation and wind scenarios together with models of oil aging and behavior. These simulations were reactive responses to this specific spill incident. However, given future prospects for increased economic exploitation of the marine environment for energy [*Broder*, 2010] and other resource needs, it seems plausible that, although safety will no doubt improve, future incidents may occur that again cause concern to coastal communities

Monitoring and Modeling the *Deepwater Horizon* Oil Spill:
A Record-Breaking Enterprise
Geophysical Monograph Series 195

10.1029/2011GM001125

[*Ornitz and Champ*, 2002]. In this paper, we examine a more proactive approach. It can provide coastal communities a tool to better understand their individual vulnerabilities in advance. The approach uses adjoint forms of the transport equations to yield impact assessments with quantitative uncertainties for any coastal location.

Our paper is structured as follows. We begin by outlining the adjoint approach that we will demonstrate in section 2. Then, we describe the physical transport model employed and show results that characterize its fidelity in section 3. In section 4, we present example results computed from the adjoint method. Concluding, in section 5, we summarize the lessons learned.

2. ADJOINT METHODS FOR TRANSPORT EQUATIONS

Atmospheric studies have long used adjoint approaches to understand potential sources of emission plumes [for example, *Hourdin et al.*, 1999; *Vukićević and Hess*, 2000; *Hourdin and Talagrand*, 2006; *Zhang et al.*, 2009a; *Kopacz et al.*, 2010]. In atmospheric studies, the goal is often to determine emission source locations and strengths at time t_0 that are consistent with an observed distribution of atmospheric gases at some later time t_1. In this case, the adjoint formalism provides a means to compute back trajectories that can be used to solve for emission scenarios at time t_0 that are consistent with the observed emitted quantity distribution at time t_1. In these studies, the wind circulation transports the emitted gas and mixes it in the atmosphere in a forward model that is configured to simulate the circulation and mixing for the time period $t_0 \rightarrow t_1$. The same general approach has been applied to tracer transport in the ocean as a tool for dynamical understanding [*Hill et al.*, 2004; *Fukumori et al.*, 2004; *Qu et al.*, 2009]. In these studies, a spatially and temporally varying, nondivergent, ocean circulation field $u(x,y,z,t)$ is used to transport an inert tracer $\phi(x,y,z,t)$ in a model according to an Eulerian transport equation of the form

$$\frac{\partial \phi}{\partial t} = -\mathbf{u}\cdot\nabla\phi + \nabla\cdot\kappa\nabla\phi + S_\phi, \tag{1}$$

where κ is the mixing tensor for a diffusive subgrid scale closure that represents unresolved mixing and ensures numerical stability. The term S_ϕ represents any source or sink terms for the tracer.

Equation (1) can be used to evaluate, for a given source location and flow field, where a tracer will be transported to. This is the approach used in the forward experiments we describe in section 3 and in the work reported by *Adcroft et al.* [2010], *Maltrud et al.* [2010], and elsewhere. A second question to ask is: For a given flow field and location, what source site injections at an earlier time t_0 would be transported to that location by time t_1. This second question can be addressed through the adjoint model counterpart of equation (1). We can formalize this question mathematically by defining a cost function J that is the mean concentration of tracer ϕ at a particular location or region Ω and at a particular time or time period, $t_a \le t \le t_b$, so that

$$J = \frac{1}{\Gamma}\int_{t=t_a}^{t=t_b}\int_\Omega \phi(x,y,z,t)\mathrm{d}x\mathrm{d}y\mathrm{d}z\mathrm{d}t, \tag{2}$$

where $\Gamma = \int_{t=t_a}^{t=t_b}\int_\Omega \mathrm{d}x\mathrm{d}y\mathrm{d}z\mathrm{d}t$. The question posed can then be expressed in terms of calculating a partial derivative, $\partial J/\partial\phi(x,y,z,t)$, which gives the sensitivity of J with respect to tracer concentrations at all locations and times.

2.1. Adjoint Equation Derivation

As described by *Errico* [1997], *Marotzke et al.* [1999], and others, we can compute $\partial J/\partial\phi(x,y,z,t)$ numerically using the adjoint equations corresponding to equation (1). Note that *Moore et al.* [2009] and *Zhang et al.* [2009b] provide alternative ways of explaining adjoint sensitivity than presented here. If we define Ω appropriately (for example corresponding to a section of coastline), then numerical evaluation of $\partial J/\partial\phi(x,y,z,t)$ will provide time-dependent spatial maps showing where and to what degree tracer injections at an earlier time would impact the region defined by Ω. Using this approach, we can evaluate for any region Ω the "envelope" of locations that have the potential to impact that region.

To derive the equation for computing $\partial J/\partial\phi(x,y,z,t)$, we first consider a discrete form of equation (1), which we can write as

$$\phi^{n+1} = \mathcal{L}^n(\phi^n, \mathbf{S}^n, \kappa^n, \mathbf{u}^n), \tag{3}$$

or more abstractly as

$$\mathbf{q} = \mathcal{L}^n(\mathbf{p}), \tag{4}$$

where ϕ^n, S^n, κ^n, and u^n are vectors of real numbers representing a discrete model state at time step n, and $\mathcal{L}^n$ is a function that steps ϕ to time level $n+1$ according to equation (1). These numbers are combined into a single vector p in equation (4) for which we can write the Jacobian matrix as

$$\mathbf{L}^n = \begin{bmatrix} \frac{\partial q_1}{\partial p_1} \frac{\partial q_1}{\partial p_2} \cdots \frac{\partial q_1}{\partial p_m} \\ \vdots \\ \frac{\partial q_m}{\partial p_1} \frac{\partial q_m}{\partial p_2} \cdots \frac{\partial q_m}{\partial p_m} \end{bmatrix}. \tag{5}$$

where m is the total number of elements in $\mathbf{p}$. The Jacobian, $\mathbf{L}^n$ gives the linear response, $\delta\mathbf{q}$, of the system to a perturbation $\delta\mathbf{p}$ such that

$$\delta\mathbf{q} = \mathbf{L}^n\delta\mathbf{p} \tag{6}$$

for a single time step and

$$\delta\mathbf{q} = \mathbf{L}^{n+k-1}\ldots\mathbf{L}^{n+1}\mathbf{L}^n\delta\mathbf{p} \tag{7}$$

for multiple time steps. This represents the forward sensitivity, or tangent linear model, for equation (1). Assuming that the terms $\frac{\partial q_i}{\partial p_j}$ in $\mathbf{L}$ can be computed, then equation (6), or more generally equation (7), can be used to compute forward sensitivities. For example, if we set $\delta\mathbf{p}_i = 1$ for a single element i of $\delta\mathbf{p}$, and $\delta\mathbf{p}_j = 0$ for $j \neq i$, then evaluating equation (6) will yield a vector of numerically evaluated partial derivatives

$$\delta\mathbf{q} = \begin{pmatrix} \frac{\partial q_1}{\partial p_i} \\ \vdots \\ \frac{\partial q_m}{\partial p_i} \end{pmatrix}. \tag{8}$$

This vector gives a numerical measure of the linearized change that a unit perturbation in element i induces in every other vector element for step n of our model. Applying $\mathbf{L}$ for subsequent time steps, as in equation (7), will show how this perturbation propagates over multiple steps.

Again, assuming we can compute $\mathbf{L}$ somehow, the adjoint technique we are interested in here makes use of its transpose ${}^t\mathbf{L}$. Multiplying ${}^t\mathbf{L}$ on a perturbation vector, $\delta\tilde{\mathbf{p}}$, with $\delta\tilde{\mathbf{p}}_i = 1$ and $\delta\tilde{\mathbf{p}}_j = 0$ for $j \neq i$ will yield a vector

$$\delta\tilde{\mathbf{q}} = \begin{pmatrix} \frac{\partial \tilde{q}_i}{\partial \tilde{p}_1} \\ \vdots \\ \frac{\partial \tilde{q}_i}{\partial \tilde{p}_m} \end{pmatrix}. \tag{9}$$

The $\delta\tilde{\mathbf{q}}$ vector gives a numerical measure of the linearized change in element i that a unit perturbation in each element of $\delta\tilde{\mathbf{p}}$ would produce.

As in equation (7), the adjoint approach can be applied over multiple steps by evaluating

$$\begin{aligned} \delta\phi^{\mathbf{n}} &= {}^t(\mathbf{L}^{n+k-1}\ldots\mathbf{L}^{n+1}\mathbf{L}^n)\delta\phi^{\mathbf{n+k}} \\ &\equiv {}^t\mathbf{L}^n{}^t\mathbf{L}^{n+1}\ldots{}^t\mathbf{L}^{n+k-1}\delta\phi^{\mathbf{n+k}}, \end{aligned} \tag{10}$$

where we have used the identity $(\mathbf{ABC})^T \equiv \mathbf{C}^T\mathbf{B}^T\mathbf{A}^T$. However, unlike equation (7), the adjoint multistep form requires applying the individual Jacobian matrix transposes in reverse order, starting at the Jacobian for the final step of the model and working backward. As with the tangent linear model in equation (7), we can apply the adjoint model not just to a single point perturbation but to any vector we can define. In particular, we can define a model step that collects terms for the integral in equation (2).

2.1.1. Adjoint of transport equation. Computation of $\mathbf{L}$ and ${}^t\mathbf{L}$ for the transport in equation (1) can be derived from its discrete form as follows. In one dimension, we can express a very simple, forward-time central-space discrete form of the advection term, $\mathbf{u}\cdot\nabla\phi$, in equation (1) as

$$\phi_i^{n+1} = \phi_i^n - \frac{u\Delta t}{2\Delta x}(\phi_{i+1}^n - \phi_{i-1}^n), \tag{11}$$

where Δt and Δx are the discrete model time step and spatial grid size, respectively, and i is the grid cell index. The Jacobian for this operation will then have the form

$$\mathbf{L}^n = \begin{bmatrix} \ddots & \ddots & \ddots & 0 & \cdots & \cdots \\ 0 & \frac{u\Delta t}{2\Delta x} & 0 & -\frac{u\Delta t}{2\Delta x} & 0 & \cdots \\ \cdots & 0 & \frac{u\Delta t}{2\Delta x} & 0 & -\frac{u\Delta t}{2\Delta x} & 0 \\ \cdots & \cdots & 0 & \ddots & \ddots & \ddots \end{bmatrix} + \mathbf{I}, \tag{12}$$

reflecting the linear nature of the equation. The adjoint (or transpose) of $\mathbf{L}$ is simply the advection term in equation (1) with the sign reversed so that the transformation $\mathbf{u}\cdot\nabla\phi \rightarrow -\mathbf{u}\cdot\nabla\phi$ gives the adjoint of the advection term. This transformation will hold for any advection scheme for nondivergent flow that uses a flux form in which the flux into one discrete model cell always equals minus the flux into the adjacent cell. The advection schemes used in our numerical experiments are of this class.

2.1.2. Adjoint of mixing equation. A similar analysis to that in section 2.1.1 can be applied to the mixing term $\nabla\cdot\kappa\nabla\phi$ in equation (1). In a simple 1-D form, with a constant value for the elements of κ, the mixing equation can be written

$$\phi_i^{n+1} = \phi_i^n + \frac{\kappa\Delta t}{\Delta x^2}(\phi_{i+1} + \phi_{i-1} - 2\phi_i). \tag{13}$$

This leads to an adjoint Jacobian operator ${}^t\mathbf{L}^{\mathbf{n}}$ and tangent linear operator $\mathbf{L}^{\mathbf{n}}$ that are identical such that

$$\mathbf{L}^n = {}^t\mathbf{L}^n = \frac{\kappa\Delta t}{\Delta x^2}\begin{bmatrix} \ddots & \ddots & \ddots & 0 & \cdots & \cdots \\ 0 & 1 & -2 & 1 & 0 & \cdots \\ \cdots & 0 & 1 & -2 & 1 & 0 \\ \cdots & \cdots & 0 & \ddots & \ddots & \ddots \end{bmatrix} + \mathbf{I}. \tag{14}$$

This relation holds for the mixing schemes used in the numerical experiments we describe, so that the adjoint form for our mixing term is simply the mixing term applied to our adjoint variables.

3. FORWARD MODEL SETUP AND RESULTS

The simulations described here were performed using the Massachusetts Institute of Technology General Circulation Model (MITgcm) on a subdomain of a cubed sphere grid. The MITgcm is a configurable general circulation model developed at Massachusetts Institute of Technology [see e.g., *Marshall et al.*, 1997; *Marotzke et al.*, 1999; *Adcroft et al.*, 2004] and, in collaboration with NASA-JPL, was used to generate the ECCO2 global ocean synthesis [*Menemenlis et al.*, 2008].

The ECCO2 global synthesis uses a Cubed Sphere 510 (CS510) resolution grid (nominally about 20 km resolution), has 50 vertical levels (with 20 levels in the top 300 m), and provides observationally constrained currents, temperature, and salinity as well as wind, heat, and precipitation at the surface for the years 1992 through 2007. Figure 1a shows a snapshot of ECCO2 current speed. The 3 day averaged ECCO2 dynamical variables are interpolated in time to 20 min and space to drive a regional subdomain with Cubed-Sphere 2040 (CS2040) resolution (nominally about 5 km resolution) using the MITgcm's Relaxing Boundary Condition Scheme (RBCS) package (see Section 6.3.2 of *MITgcm Group* [2011]). The regional CS2040 subdomain, which has the same vertical resolution as the ECCO2 synthesis, is from 100°W to 57°W and 14°N to 43°N, covering the Gulf of Mexico and western North Atlantic, as shown in Figure 1b. Note that the bathymetry in the CS2040 regional subdomain is the same as in ECCO2. A description of the numerics can be found in Appendix C of the work of *Tulloch et al.* [2011]. Both the CS510 and CS2040 model setups have 50 vertical levels with a near surface grid spacing of 10 m.

A 16 member ensemble was created from each of the years in the ECCO2 synthesis. (Note that in the calculations presented here, the "spinup" years 1992 and 1993, as well as 2007, which only runs until 31 December, have been neglected.) From 20 April to 15 July of each year (i.e., each ensemble member), floats and a buoyant passive dye tracer were injected at the site of the *Deepwater Horizon* drilling platform at a rate of 1 float per hour (2088 floats total) and 1 unit of dye per hour. These floats and dye are passively advected until the following 20 April, when they are removed. Note that subsurface plumes are not modeled here and that the floats and buoyant passive tracer are a greatly simplified model of a real oil slick at the surface. Real oil slicks are subject to, for example, environmental and biological degradation, chemical dispersal, clumping, and mixing in the water column.

Spreading statistics are computed for both the Eulerian dye, to validate the model setup against previous results, and the Lagrangian floats, to compare Lagrangian formulation with the Eulerian spreading of the dye and confirm that the numerical diffusion κ in equation (1) is negligible on time scales of a few months. Figure 2 shows an example of spreading of dye and floats in 1995. The floats are marked by red dots, and dye concentration is normalized by the current maximum. The colormap is cutoff at 0.5, and values less than 0.01 times the current maximum are white. Figures 2a and 2b are during the tracer release, and Figure 2c is shortly after the end of the release, so the maximum tracer concentration is near the *Deepwater Horizon* site. Figure 2d shows the tracer about a month and a half after the release ended. The floats track the spread of the tracer in the early stages, and the concentration of floats in Figure 2d appears to closely match the tracer concentration.

Rather than binning floats and tracer concentration for a direct comparison between float density and tracer concentration, two spreading metrics defined in the work of *Maltrud et al.* [2010] were computed using the floats for one and the tracer for the other. The first metric is the fraction of floats that exited the Gulf of Mexico at 81°W, motivated by the large

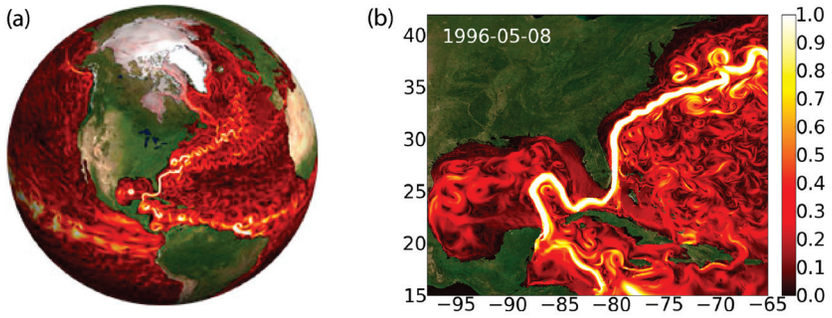

Figure 1. (a) A snapshot of current speed (m s^{-1}) from the ECCO2 global synthesis, which is on a CS510 grid (nominal resolution about 20 km). (b) A snapshot of current speed on the subdomain used for the model here, which is on a CS2040 grid (nominal resolution 5 km).

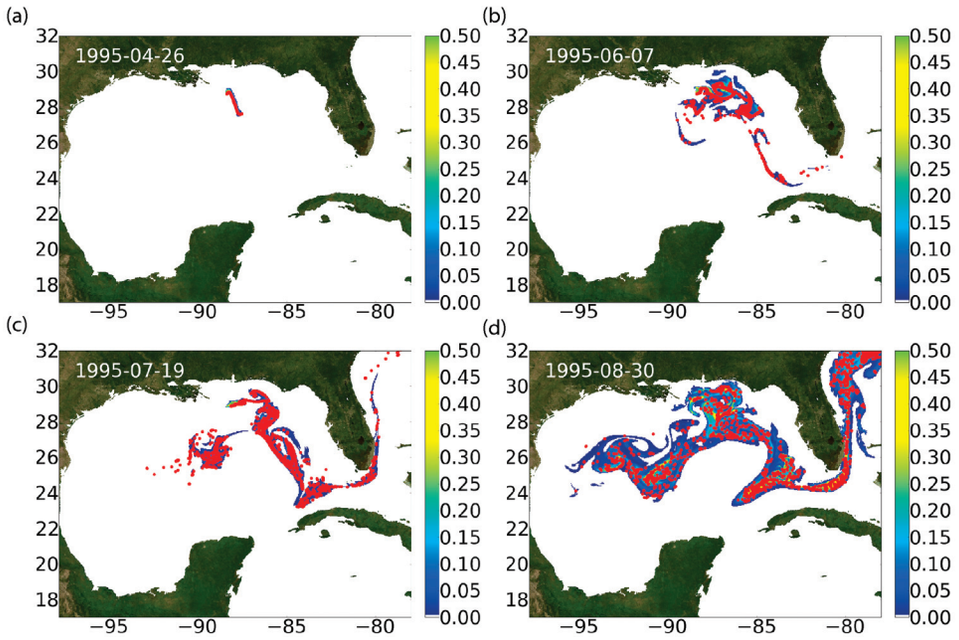

Figure 2. Snapshots of tracer (blue/green/yellow colormap) and floats (red dots) released on 20 April 1995. At each time, the tracer is normalized by its maximum, and the colormap is white for values less than 0.01 times the current maximum.

fraction of the tracer and floats that entered the Florida Straits shortly after the release (Figure 2d). The location of the *Deepwater Horizon* platform makes this metric quite sensitive to the state of the Loop Current. If an eddy has recently broken off of the Loop Current, then most of the floats will be carried slowly westward in the eddy. However, if the Loop Current is intact, then a significant fraction of the floats can be carried into the North Atlantic within a few weeks.

Figure 3b shows the fraction of floats east of 81°W. Gray lines indicate each of the ensemble years, and the thick black line is the ensemble mean. In some years, 40% of the floats have left the Gulf of Mexico by day 100, while in other years, barely any float has exited by 100 days. The ensemble mean is comparable to Figure 3 of the work of *Maltrud et al.* [2010], which shows tracer first exiting the Gulf of Mexico after 1 month, and about 45% of the ensemble mean dye exited after 6 months. Figure 3a shows the fraction of floats beyond a given radius after 40 days, which indicates that about half of the floats are likely to spread beyond 200 km from the *Deepwater Horizon* site after 40 days.

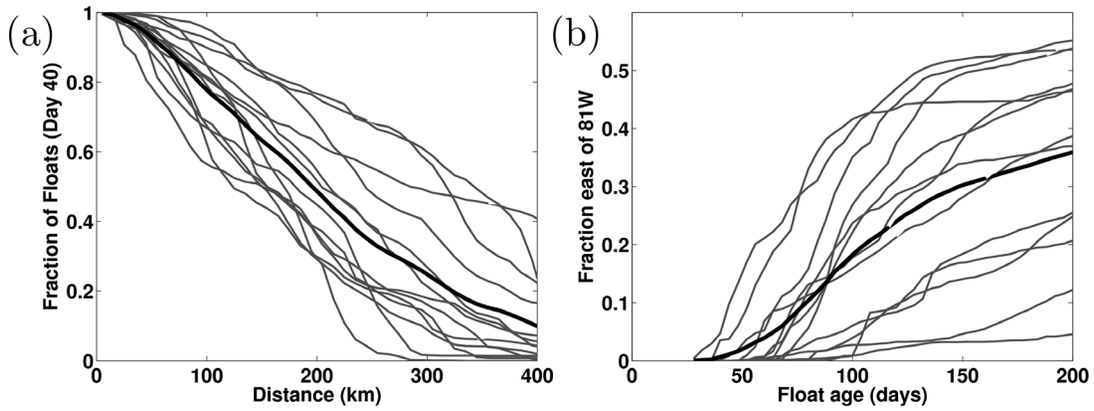

Figure 3. (left) Float fraction beyond a particular radius (on day 40), (right) fraction of floats east of the Florida Straits. Gray lines indicate individual years and the thick black line is the ensemble mean.

3.1. Relative Exposure

The second spreading metric defined in the work of *Maltrud et al.* [2010] is the "relative exposure" δ, which is the ratio of the amount of tracer seen by a water column divided by the total amount of tracer injected at the source (in *Maltrud et al.* [2010], the relative exposure was called the "dilution factor"). That is, $\delta(x,y,\tau)$ is defined as

$$\delta(x,y,\tau) \equiv \frac{\sum_{t=0}^{\tau} C(x,y,t)\,dV(x,y)}{\sum_{t=0}^{\tau} S(t)}, \qquad (15)$$

the amount of tracer from 20 April to τ days later, where $C(x, y, t, \tau)$ is the tracer concentration, dV the volume of the grid cell at (x,y), and $S(t)$ is the amount injected at the source at time t. Note that there is an implicit summation over volume in equation (15). Also note that the relative exposure is not an instantaneous measure of relative tracer concentration, which is significantly smaller away from the spill site. Tracer that passes through a grid cell or bin is summed and remembered for all future times.

Figure 4a shows the ensemble mean arrival times (in days), of tracer to a relative exposure of 0.01, with mean arrival times longer than 198 days shaded white. Arrival times were computed for each ensemble member gridpoint by summing all the days, starting at 20 April of the ensemble member's year, that $\delta < 0.01$, up to a maximum of 350 days. Since δ depends on the volume of the grid cells, binning is necessary to compare different models and grid resolutions. Figure 4c shows the ensemble mean arrival times to 0.01 relative exposure when four adjacent grid cells are binned as one 20 km wide bin. The relative exposure depends on bin size because the amount of tracer in a given water column increases while the total amount of injected tracer is fixed, so the pattern of spreading is more relevant than the magnitude of the relative exposure. The pattern in Figure 4c is similar to

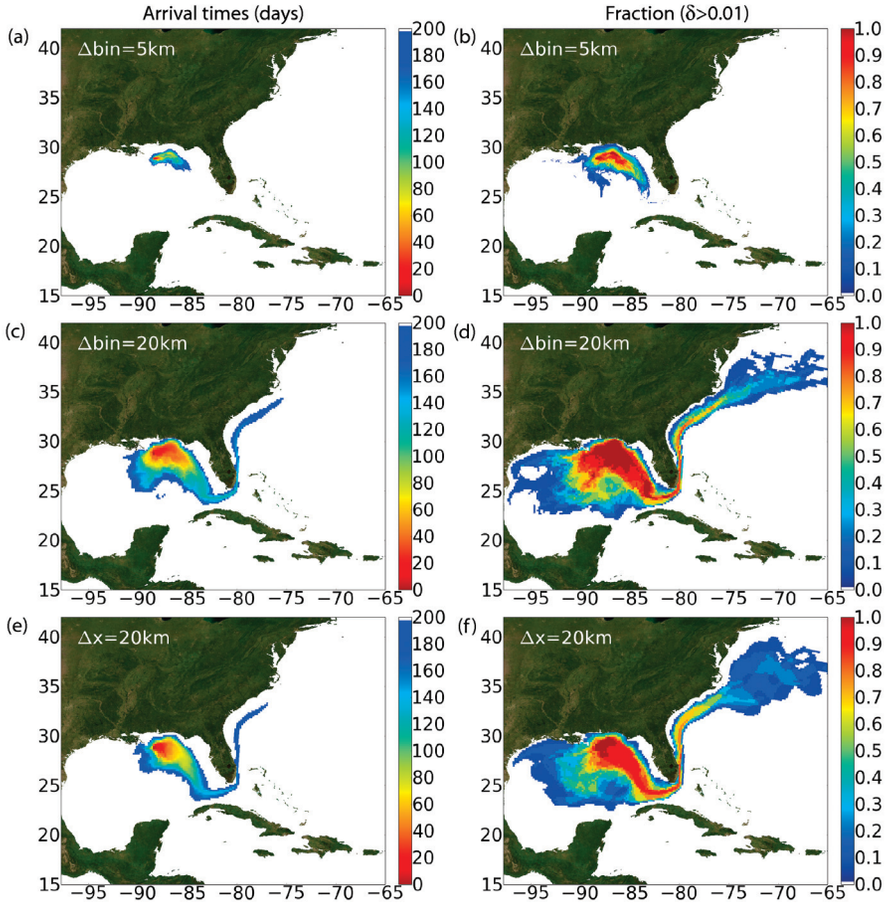

Figure 4. (left) Ensemble mean arrival times of "relative exposure" in days and (right) fraction of ensemble members reaching a relative exposure of 0.01 after 190 days. (a) and (b) are at 5 km resolution, (c) and (d) 5 km resolution binned into 20 km bins, and (e) and (f) are at 20 km resolution.

Figure 1 in the work of *Maltrud et al.* [2010], despite their grid resolution being only 10 km. The spill is expected to mostly travel east from the *Deepwater Horizon* site, which is perhaps not surprising considering the direction of the time mean Loop Current.

Figures 4b and 4d show the fraction of ensemble members that have reached a relative exposure of at least 0.01 within 190 days, which is comparable to Figure 2 of the work of *Maltrud et al.* [2010]. About 10%–20% of the ensemble members spread a fraction of the dye west toward Texas, hinting at the capacity of westward propagating eddies shed from the Loop Current to inhibit the tracer from entering the Loop Current. Analysis by *Liu et al.* [this volume(a)] indicates that multiple eddy detachments and re-attachments occurred in 2010, inhibiting oil from reaching Florida.

3.2. Sensitivity to Resolution

In this section, the ensemble of float and tracer release experiments is repeated at the original CS510 (20 km) resolution of ECCO2 and compared with the CS2040 (5 km resolution) experiments. The relative exposure metrics for the CS510 simulations are plotted in Figures 4e and f and show that at least in the ensemble mean, these metrics are fairly insensitive to model resolution.

Figure 5 shows the same float metrics as Figure 3 but for the CS510 ensemble. Again, the ensemble means (thick black line) are quite similar between the two resolutions. However, the interannual variability in the CS510 ensemble is much larger than in the CS2040 ensemble, indicating an all-or-nothing stirring depending on the state of the Loop Current. Figure 6 shows a year-by-year comparison between the high-resolution and low-resolution ensembles. Floats exiting the Gulf of Mexico via the Florida Straits after 100 days (top) in the low-resolution ensemble are apparently uncorrelated with the high-resolution ensemble up to the year 2000. Similarly in the local spreading metrics (middle and bottom panels), the low-resolution ensemble shows significantly higher interannual variability, with 1997 and 1998 having all of the floats outside 100 km at 20 days and 200 km at 40 days, while in 2002, none of the floats reached those radii. The fraction of floats outside 100 km at day 20 is not well correlated with the fraction east of 81°W in the CS510 ensemble, so despite its ensemble mean statistics appearing quite similar to the

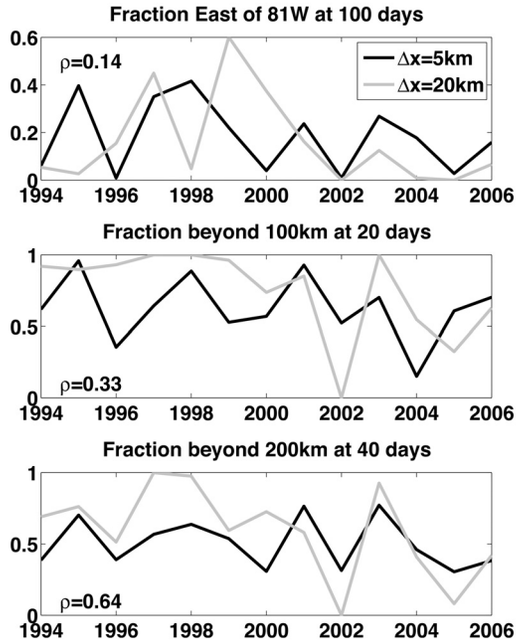

Figure 6. Year-by-year comparison of spreading metrics between CS510 ensemble (gray lines) and CS2040 ensemble (black lines).

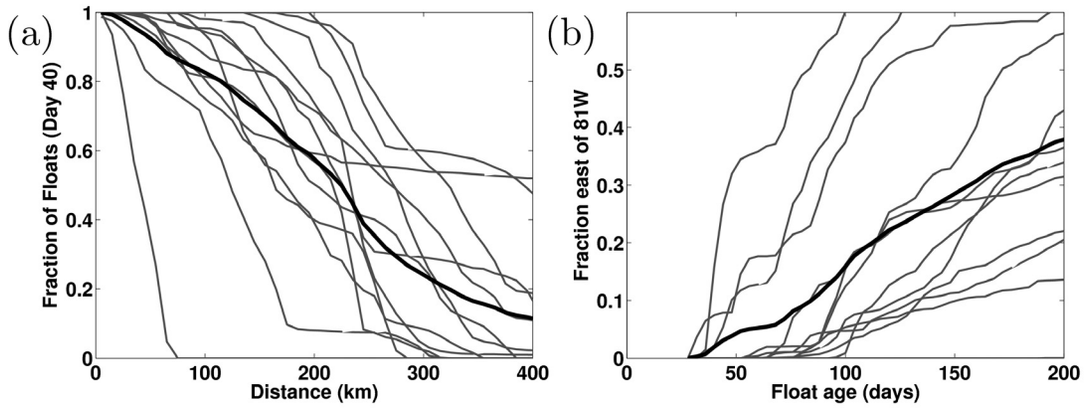

Figure 5. (left) Float fraction beyond a particular radius (on day 40), (right) fraction of floats east of the Florida Straits for CS510 resolution ensemble. Gray lines indicate individual years, and the thick black line is the ensemble mean.

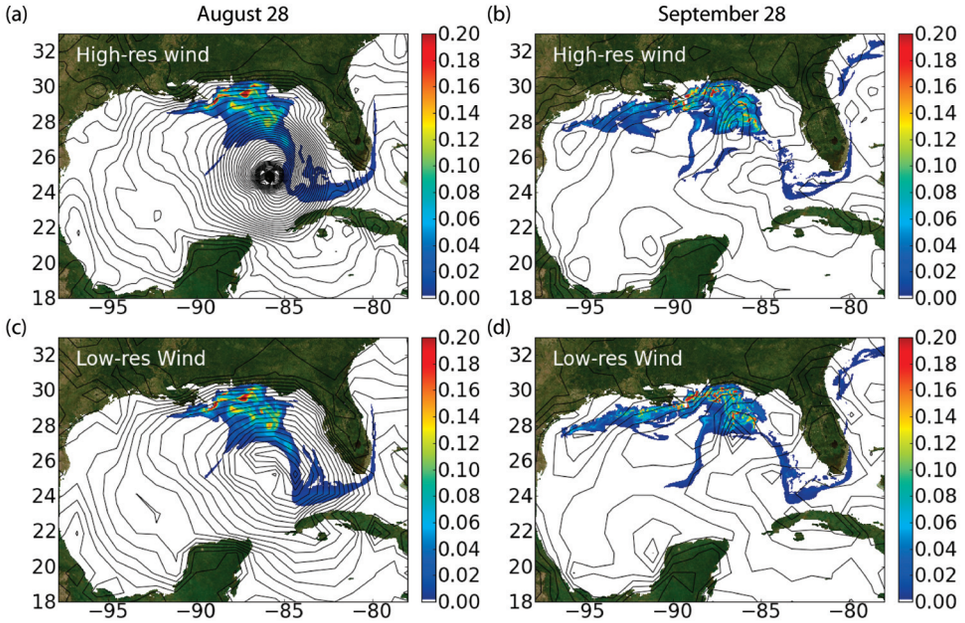

Figure 7. (left) Tracer distribution for late August 2005 and (right) 1 month later, for (top) high-resolution winds and (bottom) low-resolution winds. Wind speed is contoured in 1 m s^{-1} intervals in white.

CS2040 ensemble mean statistics, the CS510 resolution appears insufficient to adequately capture interannual variability.

Figure 7 shows the effect, or lack thereof, of high-resolution hurricane winds (top row) versus the low-resolution ECCO2 winds (bottom row) on tracer concentration before and after Hurricane Katrina in 2005. Note that wind contours (black lines) are equally spaced by 1 m s^{-1}. The high-resolution wind fields are provided on a 3 hourly and 6 km resolution grid from NOAA's H*WIND product (available at http://www.aoml.noaa.gov/hrd/data_sub/wind.html) and are nested within the 125 km resolution ECCO2 winds when and where they are available. The ECCO2 winds contain a weakened, low-resolution version of Hurricane Katrina. These low-resolution winds appear to break up the tracer into finer scale structures as it passes (from the left panels to the right panels). Fine scale winds (top) appear, however, to have little lasting impact on the tracer distribution, for example, 1 month later in Figure 7.

4. BACKWARD INTEGRATION: ADJOINT SENSITIVITY EXPERIMENT

Applying the approach outlined in section 2 to the forward model configuration examined in section 3 allows to ask the question, What is the vulnerability of any region of coastline to an offshore buoyant plume source? For each region, a cost function J is defined as in equation (2). An adjoint integration that runs from $t = t_{\mathrm{END}}$ to $t = t_{\mathrm{START}}$ is then performed using saved flow fields $u(x, y, z, t)$. As explained in section 2, the adjoint integration proceeds much like the forward simulations described in section 3 except that the sign of the flow field is reversed and the discrete model executes with time reversed, becoming

$$\frac{\partial \tilde{\phi}}{\partial(-t)} = \mathbf{u}\cdot\nabla\tilde{\phi} + \nabla\cdot\kappa\nabla\tilde{\phi} + S_{\phi} \tag{16}$$

with initial conditions $\left(\tilde{\phi} = \frac{\partial J}{\partial \phi}\right)$, where J is as defined in equation (2). The variable $\tilde{\phi}$ is the adjoint model counterpart of ϕ in equation (1). Its discrete numeric values $\tilde{\phi}(x, y, z, t)$ in a model give the sensitivity of the cost function J to perturbations in ϕ in equation (1) as a function of location (x,y,z) and time t.

4.1. Regional Cost Function Sensitivities

To illustrate the adjoint approach, we defined cost functions corresponding to three locations on the eastern coast of North America. The J_{NC} cost function is defined adjacent to Cape Hatteras on the North Carolina section of the east coast, J_{FL} is a line across the Florida Straits, and J_{LA} corresponds to the Mississippi Delta region. Note that these coastlines serve as illustrative examples of our approach. In practice, coastline cost functions would likely be defined according to exposure levels. Figure 8 shows the buoyant source sensitivities for each cost function region, J_{NC}, J_{LA}, and J_{FL} at 1, 30, and 180

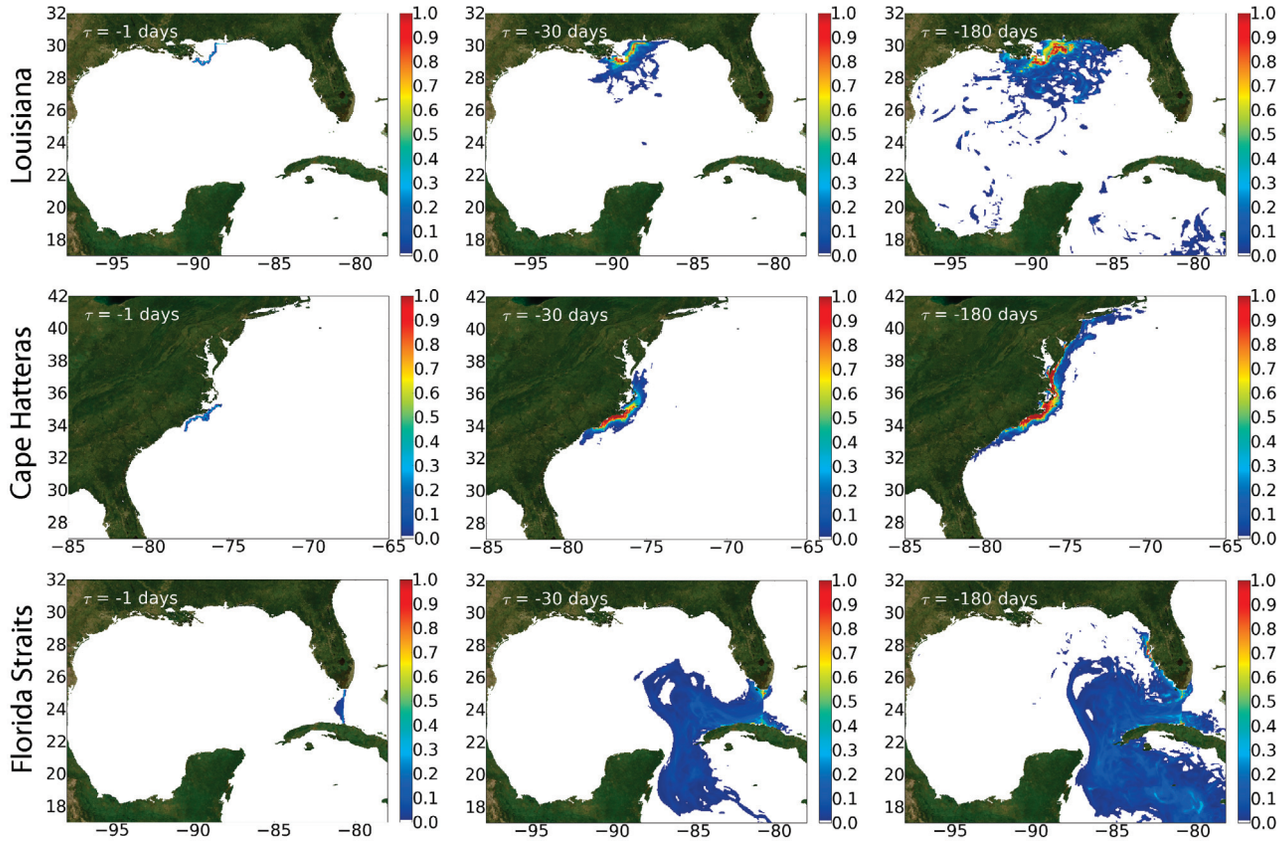

Figure 8. Adjoint sensitivity: (left to right) the ensemble mean fraction of tracer sensitivity at the "coastline" at −1, −30, and −180 days, for (top to bottom) coastal regions Louisiana, Cape Hatteras, and the Florida Straits.

days earlier. These sensitivity maps are ensemble averages of of the quantity $\tilde{\phi}$ from equation (16). The ensembles used correspond to the flow fields used in the forward experiments described in section 3. In each case, the initial value of $\tilde{\phi}$ is set to be zero everywhere except for the cost function region defined by that regions Ω. The simulation is then integrated from 180 days after April backward in time until April. The plots in Figure 8 show snapshots of $\tilde{\phi}$ at times of 1, 30, and 180 days prior to the simulation start time. This is shown for each regionally defined Ω and illustrates the envelopes of vulnerability each different Ω region implies.

Louisiana coast cost function. The top row in Figure 8 shows an Ω defined for the Louisiana coast region of the Gulf of Mexico. The plot of $\tilde{\phi}$ for $\tau = -1$ day shows the extent of the region over which J is integrated. As time progresses backward to $\tau = -30$ days, significant sensitivity spreads away from the coast. The color scale is linear with a range 0 to 1 with values below 0.01 shaded white. A value of 1 corresponds to 100% of a source in the area impacting the cost function region; a value of 0.01 corresponds to locations where 1% of the source in that region would impact the cost function region. The figure shows that a source lasting 180 days there is sensitive to most of the active drilling sites to the east of Louisiana and a region that extends well out into the deep waters in the Gulf. However, the sensitivity map also shows that sites to the west of the Louisiana coast are less likely to impact the coast than regions to the east.

North Carolina coast function. The middle row of Figure 8 shows results for Ω corresponding to the North Carolina Cape Hatteras region. This is roughly the region where the Gulf Stream separates (see Figure 1). The sensitivities do not, however, show a strong signature of propagation back along the Gulf Stream path. Instead, somewhat surprisingly, the sensitivities in the model flows examined are confined to the immediate coast, whereas the Gulf Stream separates several tens of kilometers off shore. Instead, the model shows sensitivities propagating both northeast and southwest along the coast, highlighting the along-coast currents in the model in this region. The plots show that this region has quite extensive potential sensitivity to coastal locations all along the Atlantic east coast from as far south as Georgia to as far north as Maryland, reflecting along-coast drift that varies strongly

with winds over the 180 days for which the sensitivities are computed. This illustrates how the adjoint model can be used to measure the impacts of a specific flow field.

Florida Straits cost function. The lower row shows sensitivity pathways for the Florida Straits. It shows the clear impact of the boundary current, with no sensitivity downstream in the strong Gulf Stream and extensive sensitivities upstream around the path that the Loop Current takes through the Gulf of Mexico. In a 180 day period, the sensitivities extend all the way back to the Caribbean Sea and also along the west coast of Florida.

5. CONCLUSIONS AND SUMMARY

We have examined an ensemble of ocean circulation patterns for the Gulf of Mexico and U.S. southeastern region, studying how the circulation transports a buoyant surface plume. The ensemble is taken from a time series of circulation estimates from an observationally constrained state estimate for the years 1992–2007, providing 15 different flow fields that can be used as representative of possible flows. Using these flow fields, we have calculated the transport of a buoyant plume injected at the *Deepwater Horizon* site. The transport of the plume is consistent with other studies.

Having established the flow field fidelity, we then examine adjoint computations that illustrate a proactive approach to understanding the vulnerability of any location to a spill event. Using this approach, we show that areas of most concern for the east coast of the United States do not include the *Deepwater Horizon* site. Indeed, consistent with observations, there is little evidence in either our forward or our adjoint studies that significant volumes of oil would reach the U.S. east coast from a spill at the *Deepwater Horizon* location. However, the simulations do suggest that the Cape Hatteras region would be strongly affected by a spill well to the north, as well as a spill to the south. The results we computed also suggest that the Florida Strait is much more vulnerable to pollution entering around the Florida west coast areas than it is to a spill such as the *Deepwater Horizon*.

These calculations demonstrate a future strategy in which high-resolution, historical, state estimates can be used by any location wishing to understand its vulnerability and plan accordingly. The appeal of this approach is that useful calculations can be undertaken prior to any spill incident. The results could, in principle, be computed for discrete locations all along the coast of North America using state-of-the-art circulation state estimates. This would furnish planners and responders with material with which to anticipate levels of risk in advance of any incident.

Illustrated by theses computations is an unanticipated role for multidecadal ocean state estimates derived for climate monitoring. These estimates provide the starting point for the highlighted adjoint computations and suggest another reason to sustain investments in maintaining and improving such estimates. Without accurate historical state estimates, the adjoint approaches we have described cannot be developed. In this project, we have used a global estimate, as it is broadly applicable and widely available. More detailed studies could be envisioned in which regional estimates are used which are more strongly constrained for a target region. Similarly, we have illustrated the power of this approach looking only at a single time window, running backward to April 2010. A comprehensive risk assessment for a specific location would obviously look at other time windows with as accurate a model as possible and over as long a time history as possible. This would yield the most accurate assessment of risk statistics at a location for a spill that might occur at an unknown time and location.

Acknowledgments. The ECCO2 state estimates were developed with funding from the NASA Modeling and Analysis program.

REFERENCES

Adcroft, A., C. Hill, J. Marshall, and P. Heimbach (2004), Overview of the formulation and numerics of the MIT gcm, in *Proceedings of the ECMWF: Seminar Series on Numerical Methods, Recent Developments in Numerical Methods for Atmosphere and Ocean Modelling*, pp. 139–149, Eur. Cent. for Medium-Range Weather Forecasts, Reading, U. K.

Adcroft, A., R. Hallberg, J. P. Dunne, B. L. Samuels, J. A. Galt, C. H. Barker, and D. Payton (2010), Simulations of underwater plumes of dissolved oil in the Gulf of Mexico, *Geophys. Res. Lett.*, *37*, L18605, doi:10.1029/2010GL044689.

Barker, C. H. (2011), A statistical outlook for the *Deepwater Horizon* oil spill, in *Monitoring and Modeling the Deepwater Horizon Oil Spill: A Record-Breaking Enterprise*, *Geophys. Monogr. Ser.*, doi:10.1029/2011GM001129, this volume.

Broder, J. (2010), Obama to open offshore areas to oil drilling for first time, *New York Times*. [Available at http://www.nytimes.com/2010/03/31/science/earth/31energy.html.]

Errico, R. (1997), What is an adjoint model?, *Bull. Am. Meteorol. Soc.*, *78*(11), 2577–2592.

Fukumori, I., T. Lee, B. Cheng, and D. Menemenlis (2004), The origin, pathway, and destination of Niño-3 water estimated by a simulated passive tracer and its adjoint, *J. Phys. Oceanogr.*, *34*, 582–604.

Hill, C., V. Bugnion, M. Follows, and J. Marshall (2004), Evaluating carbon sequestration efficiency in an ocean circulation model by adjoint sensitivity analysis, *J. Geophys. Res.*, *109*, C11005, doi:10.1029/2002JC001598.

Hourdin, F., and O. Talagrand (2006), Eulerian backtracking of atmospheric tracers. I: Adjoint derivation and parametrization of subgrid-scale transport, *Q. J. R. Meteorol. Soc.*, *132*(615), 567–583.

Hourdin, F., J. Issartel, B. Cabrit, and A. Idelkadi (1999), Reciprocity of atmospheric transport of trace species, *C. R. Acad. Sci., Ser. IIa Sci. Terre Planetes*, *329*(9), 623–628.

Ji, Z.-G., W. R. Johnson, and Z. Li (2011), Oil Spill Risk Analysis model and its application to the *Deepwater Horizon* oil spill, in *Monitoring and Modeling the Deepwater Horizon Oil Spill: A Record-Breaking Enterprise*, *Geophys. Monogr. Ser.*, doi:10.1029/2011GM001117, this volume.

Kopacz, M., et al. (2010), Global estimates of CO sources with high resolution by adjoint inversion of multiple satellite datasets (MOPITT, AIRS, SCIAMACHY, TES), *Atmos. Chem. Phys.*, *10* (3), 855–876.

Liu, Y., R. H. Weisberg, C. Hu, C. Kovach, and R. Riethmüller (2011a), Evolution of the Loop Current system during the *Deepwater Horizon* oil spill event as observed with drifters and satellites, in *Monitoring and Modeling the Deepwater Horizon Oil Spill: A Record-Breaking Enterprise*, *Geophys. Monogr. Ser.*, doi:10.1029/2011GM001127, this volume.

Liu, Y., R. H. Weisberg, C. Hu, and L. Zheng (2011b), Trajectory forecast as a rapid response to the *Deepwater Horizon* oil spill, in *Monitoring and Modeling the Deepwater Horizon Oil Spill: A Record-Breaking Enterprise*, *Geophys. Monogr. Ser.*, doi:10.1029/2011GM001121, this volume.

Maltrud, M., S. Peacock, and M. Visbeck (2010), On the possible long-term fate of oil released in the *Deepwater Horizon* incident, estimated using ensembles of dye release simulations, *Environ. Res. Lett.*, *5*, 035301, doi:10.1088/1748-9326/5/3/035301.

Marotzke, J., R. Giering, K. Zhang, D. Stammer, C. Hill, and T. Lee (1999), Construction of the adjoint MIT ocean general circulation model and application to Atlantic heat transport sensitivity, *J. Geophys. Res.*, *104*(29), 529–548.

Marshall, J., A. Adcroft, C. Hill, L. Perelman, and C. Heisey (1997), A finite-volume, incompressible Navier Stokes model for studies of the ocean on parallel computers, *J. Geophys. Res.*, *102*, 5753–5766.

Menemenlis, D., J. Campin, P. Heimbach, C. Hill, T. Lee, A. Nguyen, M. Schodlok, and H. Zhang (2008), ECCO2: High resolution global ocean and sea ice data synthesis, *Mercator Ocean Q. Newsl.*, *31*, 13–21.

MITgcm Group (2011), *Mitgcm User Manual*, Mass. Inst. of Technol., Cambridge. [Available at http://dev.mitgcm.org/public/r2_manual/latest/online_documents/manual.html.]

Moore, A., H. Arango, E. Di Lorenzo, A. Miller, and B. Cornuelle (2009), An adjoint sensitivity analysis of the Southern California Current circulation and ecosystem, *J. Phys. Oceanogr.*, *39*(3), 702–720.

Ornitz, B., and M. Champ (2002), *Oil Spills First Principles: Prevention and Best Response*, 1st ed., 653 pp., Elsevier, Oxford, U. K.

Qu, T., S. Gao, I. Fukumori, R. Fine, and E. Lindstrom (2009), Origin and pathway of equatorial 13 c water in the pacific identified by a simulated passive tracer and its adjoint, *J. Phys. Oceanogr.*, *39*(8), 1836–1853.

Tulloch, R. T., J. C. M. C. Hill, and K. S. Smith (2011), Scales, growth rates and spectral fluxes of baroclinic instability in the ocean, *J. Phys. Oceanogr.*, *41*, 1057–1076, doi:10.1175/2011JPO4404.1.

Vukićević, T., and P. Hess (2000), Analysis of tropospheric transport in the pacific basin using the adjoint technique, *J. Geophys. Res.*, *105*(D6), 7213–7230.

Weisberg, R. H., L. Zheng, and Y. Liu (2011), Tracking subsurface oil in the aftermath of the *Deepwater Horizon* well blowout, in *Monitoring and Modeling the Deepwater Horizon Oil Spill: A Record-Breaking Enterprise*, *Geophys. Monogr. Ser.*, doi:10.1029/2011GM001131, this volume.

Zhang, L., D. J. Jacob, M. Kopacz, D. K. Henze, K. Singh, and D. A. Jaffe (2009a), Intercontinental source attribution of ozone pollution at western U.S. sites using an adjoint method, *Geophys. Res. Lett.*, *36*, L11810, doi:10.1029/2009GL037950.

Zhang, W., J. Wilkin, J. Levin, and H. Arango (2009b), An adjoint sensitivity study of buoyancy-and wind-driven circulation on the new jersey inner shelf, *J. Phys. Oceanogr.*, *39*(7), 1652–1668.

C. Hill, O. Jahn and R. Tulloch, Department of Earth, Atmospheric and Planetary Sciences, Massachusetts Institute of Technology, 77 Massachusetts Avenue, Cambridge, MA 02139, USA. (cnh@ocean.mit.edu; jahn@mit.edu; tulloch@mit.edu)